Mathematica
Balkanica

New Series Vol. 25, 2011, Fasc. 3

Spectral Performance of RKDG Methods

V. Wheatley[1], *H. Kumar*[2] *and R. Jeltsch*[3]

The spectral properties of RKDG schemes are investigated by computing their approximate modified wavenumber behavior and by comparing numerically obtained spectra to that of an exact solution. The modified wavenumber behavior of high-order unlimited RKDG schemes is found to be excellent. In particular, the dispersive performance of the fourth-order scheme is remarkably good, with very little deviation from spectral behavior over the complete range of numerically resolved wavenumbers. The dissipation of this scheme is also very low, even at high wavenumbers. This behavior is confirmed by spectra from smooth numerical solutions. When limiting is required, however, the spectral performance of RKDG schemes tends to that of the first-order method at high wavenumbers. Thus in the vicinity of discontinuities, high-order RKDG methods exhibit high numerical dissipation due to the use of a limiter that reduces the polynomial order of the approximate solution to at most one.

1. Introduction.

To simulate flows with small-scale features such as turbulence, high-order accurate, low dissipation numerical methods are required. Runge-Kutta Discontinuous Galerkin (RKDG) methods are high-order finite element methods for nonlinear hyperbolic conservation laws, which also incorporate many features of finite volume schemes. To the best of our knowledge their dissipation properties have not been rigorously assessed. Such an analysis is important, because high order accuracy does not ensure good dissipation properties. For example, WENO schemes (see [12]) are formally high order accurate, but because they exhibit high numerical dissipation at high wave numbers, in [10]) authors find that they are not suitable for their large eddy simulations (LES).

The discontinuous galerkin methods were first introduced by Hill et al.(see [11]) for neutron transport equations (linear hyperbolic equations). In

[16] authors proved a rate of convergence of $(\Delta x)^k$ for general triangulation and of $(\Delta x)^{k+1}$ for Cartesian meshes. In case of general triangulation the result was then improved in [13] to have order of convergence of $(\Delta x)^{k+1/2}$, which was confirmed to be optimal in [18]. These methods were then generalized for system of hyperbolic conservation laws by Cockburn *et al.* in series of papers (see [2], [3], [4], [5], [6]). In DG methods, the solution is approximated by piecewise polynomial in each cell for space discretization. For the computation of the numerical flux, exact or approximated Riemann solvers from finite volume methods are used. The limiters (see [1]) are used to achieve non-oscillatory behavior of the solution, if it contains shocks. Due to this, DG methods can be seen as a generalization of finite volume methods to higher order. Due to the assumed discontinuity of the solution at element interfaces, DG methods can easily handle adaptive strategies and can be easily parallelized. For time discretization total variation diminishing (TVD) explicit Rung-Kutta (RK) methods proposed by [21] are used. These methods are known as Runge-Kutta Discontinuous Galerkin (RKDG) methods.

One quantity that can be used to assess the spectral properties of a scheme is the modified wavenumber. The imaginary part of the modified wavenumber provide information related to the spectral dissipation, whereas the real part provide information about the spectral dispersion of the numerical scheme.

While the modified wavenumber contains a wealth of information on the spectral properties of a spatial discretization scheme, it is not always possible to analytically compute the modified wavenumber for all schemes. Notably, shock capturing schemes use conservative approximations for the spatial derivative,

$$u'_j = \frac{1}{h}(\tilde{u}_{j+1/2} - \tilde{u}_{j-1/2}),$$

that require the definition of numerical fluxes $\tilde{u}_{j\pm1/2} = \tilde{u}(u_{j-q+1}, \ldots, u_{j+r})$. The flux function $\tilde{u}$ is generally a nonlinear function of its arguments even for linear equations, due to limiting. This nonlinearity prohibits the analytical calculation of the modified wavenumber. However, for nonlinear schemes, Pirozzoli in [19] has devised a method to compute the approximate modified wavenumber behavior numerically. As RKDG methods also use nonlinear limiting, we will use the approximated modified wavenumber to investigate the spectral performance of the RKDG methods.

This article is organized as follows: In the following Section 2 we present the ideal MHD equations. In Section 3 we describe the variational formulation for the DG methods and RK time-stepping. In Section 4 we introduce the approximated modified wavenumber for the nonlinear schemes. In Section 5 we investigate the dissipation and dispersion of the RKDG methods by computing

the approximated modified wavenumber of an isolated Fourier mode. We also analyze the effects of the limiters. We then compare these results with other shock-capturing schemes. In Section 6 we first present the convergence rates of the RKDG methods using the smooth solution of a simple wave problem. We then analyze the spectra of a simple wave to investigate the spectral performance of the RKDG methods in nonlinear simulations.

2. Governing equations

The governing equations for the simulations presented here are the ideal MHD equations. The equations of ideal MHD govern the evolution of a quasi-neutral conducting fluid and the magnetic field within it, neglecting the magnetization of individual particles, the hall current, ion slip and the time rate of change of the electric field in Maxwell's equations. The complete details about these equations can be found in [9].

The ideal MHD equations are a system of hyperbolic partial differential equations. Numerical discretization of these equations is complicated task due to the presence of nonlinearities in the convection flux. In conservative form, they can be written as

$$\frac{\partial \rho}{\partial t} + \nabla \cdot (\rho \mathbf{v}) = 0, \tag{1a}$$

$$\frac{\partial (\rho \mathbf{v})}{\partial t} + \nabla \cdot \left(\rho \mathbf{v}\mathbf{v} - \mathbf{B}\mathbf{B} + \left(p + \frac{1}{2}|\mathbf{B}|^2 \right) \right) = 0, \tag{1b}$$

$$\frac{\partial \mathbf{B}}{\partial t} + \nabla \times (\mathbf{v} \times \mathbf{B}) = 0, \tag{1c}$$

$$\frac{\partial E}{\partial t} + \nabla \cdot \left((E + p)\mathbf{v} + \left(\frac{1}{2}|\mathbf{B}|^2 \mathbf{I} - \mathbf{B}\mathbf{B} \right) \cdot \mathbf{v} \right) = 0 \tag{1d}$$

$$\nabla \cdot \mathbf{B} = 0. \tag{1e}$$

The plasma is assumed to be ideal with constant specific heats, allowing the following equation of state to be used to close the set of equations:

$$E = \frac{p}{\gamma - 1} + \frac{1}{2}\rho |\mathbf{v}|^2 + \frac{1}{2}|\mathbf{B}|^2. \tag{2}$$

Here ρ is the density, $\mathbf{v}$ is the velocity, Here ρ is the density, $\mathbf{v}$ is the velocity, p is the pressure, $\mathbf{B}$ is the magnetic field, E is the total energy of the plasma. The Eqn. (1a) is the equation for the mass conservation. Eqns. (1b)-(1d) are equations of balance laws for the momentum, the magnetic field and the total energy respectively. Eqn. (1e) is the divergence free condition for magnetic field representing nonexistence of magnetic monopoles.

Eqns. (1) can be written in conservation form as follows:

$$E = \frac{p}{\gamma - 1} + \frac{1}{2}\rho|\mathbf{v}|^2 + \frac{1}{2}|\mathbf{B}|^2. \tag{3}$$

where the vector of conserved variables $U \equiv U(x_i, t)$ is

$$U = \{\rho, \rho v_i, B_i, E\}^T,$$

and the flux vectors $F_j(U)$ are

$$F_j(U) = \Big\{ \rho v_j \, , \, \rho v_i v_j + (p + \frac{1}{2} B_k B_k)\delta_{ij} - B_i B_j \, ,$$
$$v_j B_i - v_i B_j \, , \, (E + p + \frac{1}{2} B_k B_k) v_j - B_j (B_k v_k) \Big\}^T .$$

3. Runge-Kutta discontinuous-Galerkin method

For hyperbolic problems, solutions may be piecewise continuous, meaning that they are smooth in regions separated by discontinuities. This behavior is mimicked by DG methods as they allow L^2 jumps at the boundaries of subdomains even for operators of higher than first order. This allows any complete set of trial functions to be used to represent the solution on each subdomain. This is not the case in the standard Galerkin formulation where for second order operators, C^0 continuity is required across subdomains.

3.1 Variational Form Consider a domain $\Omega \in \mathbb{R}^n$. Let us define a triangulation M of Ω as a finite collection $\{E_i\}_{i=1}^m, m \in \mathbb{N}$, of non-degenerate polygons such that,

$$\bar{\Omega} = \bigcup \{\bar{E}_i, i = 1, ..., m\}, \tag{4}$$

$$E_i \bigcap E_j = \emptyset \Leftrightarrow i \neq j, \tag{5}$$

and for all $i, j \in \{1, ..., m\}, i \neq j$, the intersection $\bar{E}_i \bigcap \bar{E}_j$ is either $\emptyset$ or a vertex, edge or face of both E_i and E_j. For two-dimensional quadrilateral elements, we introduce a reference element $\Sigma \equiv [-1, 1] \times [-1, 1]$ and the mapping

$$\Psi : E \to \Sigma \tag{6}$$

that maps quadrilateral elements to the reference element. The mapping Ψ is a bilinear mapping. It is sufficient for us to consider the following generic scalar advection equation:

$$\frac{\partial u}{\partial t} + \nabla \cdot \boldsymbol{F} = 0, \tag{7}$$

where u a conserved variable and $\boldsymbol{F}$ is the inviscid flux vector. The variational form used in the RKDG method is derived by multiplying by the test function v and integrating over each element separately. After using integration by parts on the divergence term, we obtain

$$\int_E \frac{\partial u}{\partial t} v \, dx + \int_{\partial E} v \boldsymbol{n} \cdot \boldsymbol{F}(u) \, ds - \int_E \nabla v \cdot \boldsymbol{F}(u) \, dx = 0. \tag{8}$$

The flux vector $\boldsymbol{F}(u)$ in the second term must be evaluated on the boundary of the element where u may be discontinuous and thus has two possible values: u_i on the interior of the element under consideration and u_e on the exterior. To account for this, we replace $\boldsymbol{F}(u)$ with the numerical flux function $\hat{\boldsymbol{F}}(u_i, u_e)$, which can be computed taking upwind considerations into account. We refer to [23] for the description of the approximated Riemann solvers used in this article. The final variational from is derived by using integration by parts once more on the third term to eliminate the gradient of the test function,

$$\frac{\partial}{\partial t} \int_E uv \, dx + \int_{\partial E} v \left(\hat{\boldsymbol{F}}(u_i, u_e) - \boldsymbol{F}(u_i) \right) \cdot \boldsymbol{n} \, ds + \int_E \nabla \cdot \boldsymbol{F}(u) v \, dx = 0. \tag{9}$$

3.2. Basis Functions. In the RKDG method, the unknowns and data within each element are expanded in terms of a suitable set of basis functions $\phi_{pq}(\boldsymbol{x})$,

$$f(x, y) = \sum_p \sum_q a_{pq} \phi_{pq}(\xi_1, \xi_2),$$

Here, (ξ_1, ξ_2) is a local coordinate system associated with that element. The RKDG method we use is based on the Nektar code by [20],[14],[17]. The original code has been extended to include Runge-Kutta time stepping, slope limiters and accurate Riemann solvers, amongst other features. The set of polynomial basis functions used in Nektar was proposed by [8] in two dimensions and extended to three dimensions in [20].

In order for the RKDG method to be stable in the nonlinear case, we require an entropy inequality and the uniform boundedness of the total variation of the discrete solution u_h. In general, a limiter function is required for the second condition to hold. In this article we will use two limiters namely, Minmod and Less Restrictive (LR) limiter. We refer [23] for the detail description of these limiters.

3.3. Runge-Kutta time discretization. To advance solutions in time, the RKDG method uses a Runge-Kutta (RK) time marching scheme. In this report we present the results of second-, third- and fourth-order accurate RKDG schemes, thus we limit ourselves to presenting the RK schemes used in these

order	α_{il}			β_{il}		
2	1			1		
	1/2	1/2		0	1/2	
3	1			1		
	3/4	1/4		0	1/4	
	1/3	0	2/3	0	0	2/3

Table 1: Parameters for Runge-Kutta time marching schemes.

cases. For second- and third-order simulations, we use the TVD RK schemes of [22]. For fourth-order simulations we use the classic scheme.

Consider the semi-discrete ODE,

$$\frac{du_h}{dt} = L_h(u_h).$$

Let u_h^n be the discrete solution at time t^n, and let $\Delta t^n = t^{n+1} - t^n$. In order to advance a numerical solution from time t^n to t^{n+1}, the RK algorithm is as follows:

1. Set $u_h^{(0)} = u_h^n$.
2. For $i = 1, ..., k+1$, compute,

$$u_h^{(i)} = \sum_{l=0}^{i-1} \alpha_{il} u_h^{(l)} + \beta_{il} \Delta t^n L_h(u_h^{(l)}).$$

3. Set $u_h^{n+1} = u_h^{(k+1)}$.

The values of the coefficients used are shown in Table 1. For the linear advection equation, it was proved by [7] that the RKDG method is L^∞-stable for piecewise linear ($k = 1$) approximate solutions if a second-order RK scheme is used with a time-step that satisfies

$$a\frac{\Delta t}{\Delta x} \leq \frac{1}{3},$$

where a is the constant advection speed. The numerical experiments show that when approximate solutions of polynomial degree k are used, an order $(k+1)$ RK scheme must be used, which simply corresponds to matching the temporal and

spatial accuracy of the RKDG scheme. In this case the L^∞-stability condition is

$$a\frac{\Delta t}{\Delta x} \leq \frac{1}{2k+1}.$$

For the nonlinear case, the same stability conditions are used but with a replaced by the maximum eigenvalue of the system.

4. Modified wave number

Consider the one-dimensional linear advection equation on an infinite domain with a sinusoidal initial condition with wavenumber k:

$$\frac{\partial u}{\partial t} + a\frac{\partial u}{\partial x} = 0, \quad -\infty < x < \infty, \quad u(x,0) = \hat{u}_0 e^{ikx}. \tag{10}$$

Here, we assume $a > 0$. Applying separation of variables, it is clear that the exact solution to Eqn. (10) has the form,

$$u(x,t) = \hat{u}(t)e^{ikx}. \tag{11}$$

Inserting this into Eqn.(10) we obtain,

$$\frac{d\hat{u}(t)}{dt} + iak\hat{u}(t) = 0, \quad \hat{u}(0) = \hat{u}_0. \tag{12}$$

Solving this and substituting it in (11) we get,

$$u(x,t) = \hat{u}_0 e^{ik(x-at)}. \tag{13}$$

Let us now consider the semi-discrete approximation of Eqn. (10) on a uniform grid with nodes given by $x_j = jh$,

$$\frac{\partial u_j}{\partial t} + au_j' = 0, \quad u_j(0) = \hat{u}_0 e^{ikx_j}, \tag{14}$$

where $u_j(t) \approx u(x_j,t)$, u_j' is a discrete approximation of the spatial derivative and h $(= \Delta x)$ is the mesh size. If an explicit, linear finite difference approximation of u_j' is used i.e. if

$$u_j' = \frac{1}{h}\sum_{l=-q}^{r} a_l u_{j+l}, \tag{15}$$

then the exact solution $u_j(t) = \hat{u}(t)e^{ikx_j}$ applies. Inserting this into Eqn. (14) we obtain,

$$\frac{d\hat{u}(t)}{dt} + a\frac{1}{h}\sum_{l=-q}^{r} a_l e^{iklh}\hat{u}(t) = \frac{d\hat{u}(t)}{dt} + iak_{mod}(k)\hat{u}(t) = 0, \quad \hat{u}(0) = \hat{u}_0. \tag{16}$$

This is identical to the continuous semi-discrete form given in Eqn. (12) except that the wavenumber k is replaced by the modified wavenumber

$$k_{mod}(k) = \frac{1}{ih} \sum_{l=-q}^{r} a_l e^{iklh}.$$

Hence, the exact solution to the semi-discrete equation is,

$$u_j(t) = \hat{u}_0 e^{i(kx_j - k_{mod}(k)at)}.$$

For convenience we introduce the reduced wavenumber $\phi \equiv kh$ and reduced modified wavenumber $\Phi(\phi) \equiv k_{mod}(k)h$. Rewriting the above equation in terms of reduced wavenumbers, we obtain

$$u_j(t) = \hat{u}(t)e^{ikx_j} = \hat{u}_0 e^{i(\phi j - \Phi at/h)} = \hat{u}_0 e^{\Im(\Phi)at/h} e^{i(\phi j - \Re(\Phi)at/h)}. \tag{17}$$

This illustrates the effects of the modified wavenumber on the solution. $\Im(\Phi(\phi))$ contains information on the spectral dissipation properties of the scheme. If $\Im(\Phi(\phi)) > 0$, the scheme is unstable at that wavenumber, while if $\Im(\Phi(\phi)) < 0$, the scheme is dissipative. $\Re(\Phi(\phi))$ contains information on the spectral dispersion properties of the scheme. If $\Re(\Phi(\phi)) = \phi$, disturbances with that wavenumber will propagate at the correct speed in the semi-discrete evolution.

4.1. The Approximate Modified Wavenumber for Nonlinear Schemes. Following [19], consider a numerical simulation with the initial condition $u_j(0) = \hat{u}_0 e^{ij\phi_n}$ that is advanced a single, very small, timestep Δt such that the error in time integration is negligible. If the linear, semi-discrete scheme were solved exactly, Eqn. (17) can be rearranged to give the following expression for $\Phi(\phi_n)$:

$$\Phi(\phi_n) = \frac{h}{ia\tau} \log\left(\frac{\hat{u}(\phi_n;\tau)}{\hat{u}_0}\right). \tag{18}$$

For a non-linear scheme, we can use a similar expression. However, we must account for the fact that the nonlinearities produce additional Fourier modes in the numerical solution at time τ. Thus, the amplitude of the mode associated with the reduced wavenumber ϕ_n, $\hat{u}(\phi_n;\tau)$, must be extracted from the solution by means of a discrete Fourier transform (DFT). On a finite grid with nodes $j = 0, \ldots, N$, the supported Fourier modes have reduced wavenumbers $\phi_n = 2\pi n/N$ in the range $0 \leq \phi_n \leq \pi$, and the DFT of the solution at ϕ_n is given by

$$\hat{u}(\phi_n;\tau) = \frac{1}{N} \sum_{j=0}^{N-1} u_j(\tau) e^{-ij\phi_n}.$$

Using this in Eqn. (18), the following expression is obtained for the approximate modified wavenumber corresponding to ϕ_n:

$$\Phi(\phi_n) = \frac{h}{ia\tau} \log\left(\frac{\hat{u}(\phi_n;\tau)}{\hat{u}(\phi_n;0)}\right). \tag{19}$$

It is important to note that $\hat{u}(\phi_n;0)$ is the DFT of the numerical initial condition, which may differ from the exact initial condition if, for example, the initial values were converted to cell averages to initialize a finite volume method. In order to obtain the modified wavenumber behavior for the complete spectrum, simulations must be carried out for all ϕ_n.

It is important to note that in the general case, several Fourier modes of $O(1)$ amplitude will be present in a simulation. Due to the nonlinearity of shock capturing schemes, these modes will interact and thus their evolution will not be governed precisely by the approximate modified wavenumber.

5. Approximate modified wavenumber behavior of DG methods

In order to compute the approximate modified wavenumber behavior of DG methods for MHD, a series of simulations were carried out where a sinusoidal transverse magnetic field was advected with a constant velocity. The initial conditions were as follows:

$$(\rho,\, p,\, u,\, v,\, w,\, B_x,\, B_y,\, B_z) = (1,\, 1,\, 1,\, 0,\, 0,\, 0,\, \cos(2\pi n x),\, 0).$$

This differs from the approach of Pirozzoli [19], who carried out simulations of the linear advection equation. Although the exact solution to our problem is a linearly advected B_y profile, the numerical solution will differ from that produced by a discretization of the linear advection equation due to the presence of additional characteristic speeds. These alter the timestep as well as the output of most of the Riemann solvers. Our approach should give a more accurate representation of the behavior of DG methods for MHD. Our simulations were carried out on a mesh with 100 elements in the x-direction, with element centers $x_j = jh$ and $h = 0.01$. Simulations were run for $1 < n < 49$.

Let us first examine the resulting modified wavenumber behavior for unlimited second-, third- and fourth-order DG methods. In the Fig. 1, the results for unlimited DG methods are compared to the exact behavior of a spectral method and that of a first order upwind method. The behavior of the third- and fourth-order methods was computed using both the LF flux and the HLLC flux (see [23]). All the DG methods are far superior to the first order upwind scheme. The third- and fourth-order DG schemes have much better spectral properties than the second order scheme: $\Re(\Phi)$ departs significantly less from

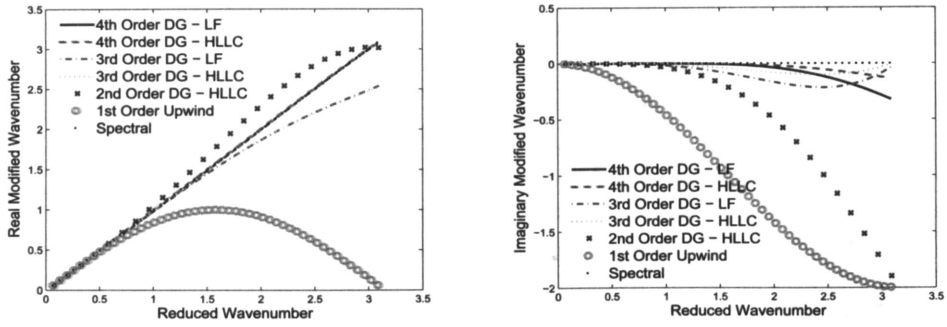

(a) (b)

Figure 1: Real (left) and imaginary (right) parts of the approximate modified wavenumber for various RKDG schemes.

spectral behavior at a much higher wavenumber for the fourth order scheme, and $\Im(\Phi)$ is significantly less negative for both third- and fourth-order schemes, indicating lower dissipation, particularly at high wavenumbers. In particular, it can be seen that the dispersive performance of the fourth-order schemes is remarkably good, with no visible deviation of $\Re(\Phi)$ from the spectral line on the scale of the plot.

The main value of these plots, however, is to observe the effect that the Riemann solver has on the spectral properties of the method. As widely claimed, the choice of Riemann solver is unimportant for high order methods. In the behavior of $\Re(\Phi)$, this claim appears to be valid; there is minimal difference in the dispersion behavior of the third order methods with the HLLC and LF fluxes. However, when we examine the imaginary part of the modified wavenumber, we see that when the HLLC flux is used, there is a very significant decrease in the dissipation at most wavenumbers for both the third- and fourth-order schemes, indicating that the choice of Riemann solver is important.

Next, we investigate the effect of limiting on the spectral behavior of DG methods. In Fig. 2 the modified wavenumber behavior of minmod and less restrictive limited (see [23]) second-order DG schemes are compared to the unlimited behavior. Initially, at low wavenumbers, the behavior of the limited schemes coincides with that of the unlimited schemes. It can be seen that the effect of the limiters is to force the scheme towards the behavior of the first-order scheme at high wavenumbers. The choice of limiter has a significant effect on the modified wavenumber of the scheme. The minmod limited scheme de-

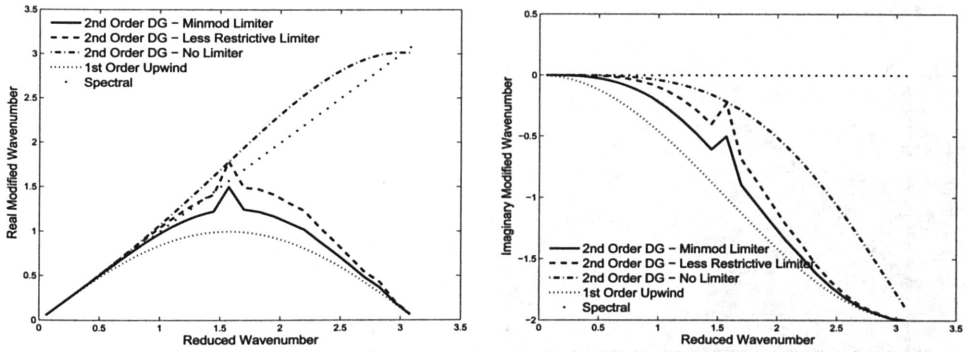

(a) (b)

Figure 2: Real (left) and imaginary (right) parts of the approximate modified wavenumber for second order limited DG schemes.

parts significantly from the behavior of the unlimited scheme at a significantly lower wavenumber than the less restrictive limited scheme. Interestingly, for the scheme with the less restrictive limiter, $\Re(\Phi) > 0$ at the lowest wavenumber, although its value is so small that it is not visible in the figure. This ndicates a linear instability of the scheme at the lowest wavenumber. Pirozzoli [19] observes similar behavior for the Superbee limited second-order finite volume scheme, and claims that the nonlinear stability properties of the scheme compensate for this.

The approximate modified wavenumber behavior obtained in [19] for various schemes is shown in Fig 3. As expected, the second-order minmod-limited finite volume and DG schemes exhibit very similar behavior. The behavior of the less restrictive-limited DG scheme resembles that of the Superbee-limited finite volume scheme. The third-order WENO behavior begins to depart significantly (by 2%) from spectral at approximately $\phi = 1.25$ for the real part, and $\phi = 0.6$ for the imaginary part. The unlimited third-order DG scheme performs much better than this, with significant departures from ideal behavior beginning at $\phi = 1.8$ and $\phi = 1.25$ for the real and imaginary parts, respectively.

The computation of the approximate modified wavenumber behavior for limited third- and fourth-order DG schemes was also attempted. However, the analysis predicted that these schemes would produce very high dissipation, even at low wavenumbers, despite the fact that the schemes should have, at worst, the same performance as the second-order scheme. The reason for this is the fact that the limiter function reduces the polynomial order of the representation of

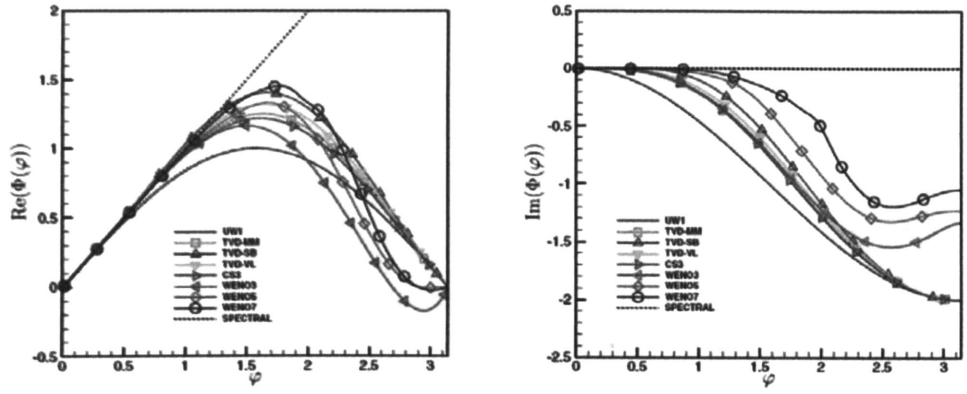

(a) (b)

Figure 3: Real (top) and imaginary (bottom) parts of the approximate modified wavenumber for the first-order upwind method (UW1), second-order TVD finite volume methods using the minmod (TVD-MM), Superbee (TVD-SB) and van Leer (TVD-VL) limiters, the third-order centered scheme (CS3), and third- (WENO3), fifth- (WENO5) and seventh-order (WENO7) WENO schemes [19].

the data to unity where ever limiting is required. For the second-order scheme, this does not cause any problems as the representation of the data is already piecewise linear. For the third- and fourth-order schemes, the data is represented by piecewise quadratic and cubic polynomials, respectively. For wavenumbers higher than $k = 1$, limiting occurs, locally reducing the polynomial order of the data from that in the numerical initial condition to unity, which constitutes a large amount of dissipation in a single timestep. For this reason we believe that the method does not produce meaningful results for schemes where maximum polynomial order of limited data does not match the order of the unlimited data.

Despite the fact that we cannot obtain meaningful results for high-order limited DG schemes, we can make the following statement: Due to the nature of the limiter used in our RKDG method, in the vicinity of discontinuities the method exhibits high numerical dissipation, similar to that of second-order finite volume methods. In this region they are inferior to high-order WENO schemes that can be seen in Fig. 3 to provide improved modified wavenumber behavior. This is because the reconstructed numerical solution is always a high-order polynomial in the WENO schemes, it is not limited to a piecewise linear function in the vicinity of discontinuities. This situation can only be improved by the development of high-order limiter functions for RKDG methods.

6. Spectral analysis for nonlinear simulations

In the previous section, we examined the approximate spectral behavior of DG schemes by isolating, as far as possible, single Fourier modes. To determine whether this approximate behavior is relevant in nonlinear simulations with a broad spectrum, we will compare the spectra from simulations of the simple wave problem described in [15] to that of the exact, non-linear smooth solution to the one-dimensional Euler equations (no magnetic field). The solution exists if the initial conditions satisfy the following relations:

$$\rho(x,0) = \rho_0 \left(1 + \frac{(\gamma-1)u_x}{2a_0}\right)^{\frac{2}{\gamma-1}},$$

$$p(x,0) = p_0 \left(1 + \frac{(\gamma-1)u_x}{2a_0}\right)^{\frac{2\gamma}{\gamma-1}},$$

$$u_y = u_z = B_x = B_y = B_z = 0.$$

The particular case we will use it with the initial velocity,

$$u_x(x,0) = u_0 \sin(\pi x),$$

on the domain $-1 < x < 1$ with the boundary condition $u(1,t) = u(-1,t)$.

6.1. Convergence for the Simple Wave Problem In Fig. 4, we show how the L_2 error in element average density converges with N for various RKDG schemes. Note that in these simulation, the LR limiter does not detect that any limiting is required, so there is no need to present separate LR limited and unlimited results. The solutions from the LR limited third-order RKDG scheme converge as the expected rate for $N \geq 16$. Solutions from the LR limited fourth-order RKDG schemes exhibit fourth-order convergence from the coarsest discretization used. On the other hand, the results from the minmod limited fourth-order RKDG scheme show an order of convergence of between one and two. This is due to the solution being limited to piecewise linear or piecewise constant on the majority of elements, once again highlighting the short-comings of this limiter.

To further investigate the importance of using accurate Riemann solvers in high-order schemes, in Fig. 4 we compare the convergence of solutions from LR limited fourth-order RKDG schemes using LF and HLLE Riemann solvers. The errors in the LF and HLLE results are indistinguishable on the scale of the plot for all discretizations used. This shows that the observation made in previous subsection, that high-order accuracy solutions to the simple wave

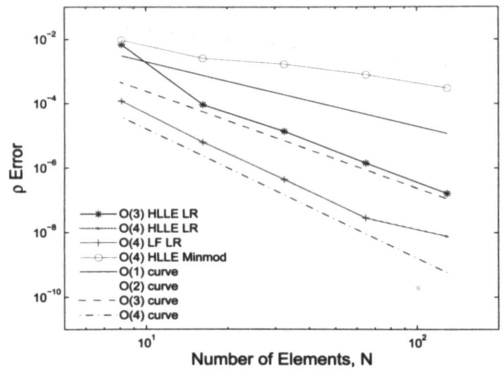

Figure 4: L_2 errors in element average density versus N for the Euler simple wave problem at $t = 0.5$.

problem are insensitive to the choice of Riemann solver, applies over a broad range of resolutions.

6.2. Spectra of Simple Wave Problem Observe that the simple wave is initially an isolated Fourier mode, as the wave steeps the spectrum becomes broad. We examine the results at $t = 0.9$, somewhat prior to the formation of a shock at $t \approx 0.95$. In Fig. 5, the solution and energy spectral density $(\hat{u}(k)^2)$ from limited second-order simulations are compared to the exact solution. The HLLC-G Riemann solver was used for both simulations. During the simulation, the less restrictive (LR) limiter did not detect that any limiting was required, thus it is unnecessary to show a separate curve for an unlimited simulation. On the other hand the minmod limiter detected that limiting was required on the majority of elements. This indicates a major short-coming of the minmod limiter for high-order simulations: The minmod limiter selects the input gradient with the minimum modulus. If this is not the gradient of the polynomial representation of the field internal to the element, then limiting is carried out and the coefficients of the higher order modes are set to zero. In the RKDG method, the input gradients are the internal gradient, and slope estimates based on the difference between the element average fields and the average fields on the adjacent elements. In general, if the solution has a finite curvature, the internal gradient will not have the minimum modulus, thus the solution will be limited and will revert to (at most) second order accuracy. This

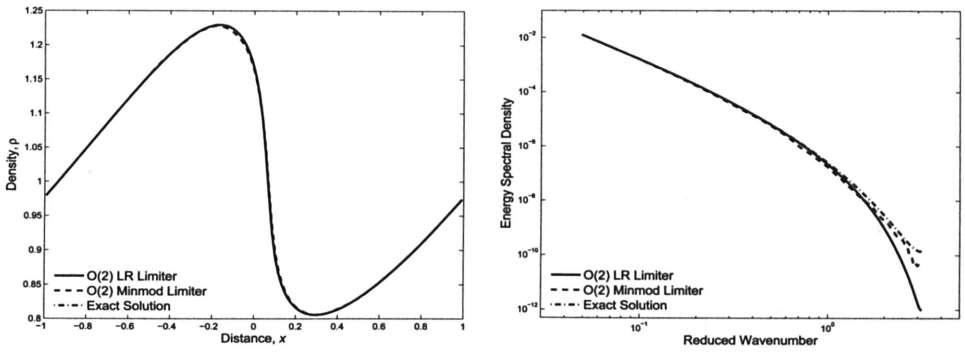

(a) (b)

Figure 5: Solutions (left) and energy spectral density (right) from second-order simulations of the Euler simple wave problem. The HLLC-G flux solver was used in all simulations shown.

will occur even if limiting is unnecessary, as is the case with the solution we are currently examining. From this we must conclude that the minmod limiter is unsuited for use in a high-order RKDG method. Examining the numerical solutions shown in Fig. 5, we see that the LR limited solution approximate the exact solution very well, while the minmod limited solution under-predicts the peak value. Examining the spectra, we see that both numerical solutions have low dissipation at low wavenumbers, while at intermediate wavenumbers the minmod limited scheme is more dissipative. This behavior is as predicted by the approximate modified wavenumber behavior. However, at the highest wavenumbers there is far less energy present in the Fourier modes from the LR limited simulation, which was not predicted. This shows that while the approximate modified wavenumber behavior is a useful guide, it cannot predict all features of a fully nonlinear simulation.

Fig. 6 shows the energy spectral density from unlimited third-order simulations using the LF, HLLE and HLLC-G Riemann solvers. The approximation of the energy spectral density is better than in the second-order simulations, with visible deviations from the exact spectrum occurring only at the highest wavenumbers. To differentiate the solutions, the relative error in this quantity,

$$\varepsilon_{\hat{u}^2}(k) = \frac{\hat{u}(k)^2_{exact} - \hat{u}_{numeric}(k)^2}{\hat{u}_{exact}(k)^2}$$

is also plotted. This shows that as predicted by the approximate modified wavenumber for unlimited third-order schemes, the LF solution is the most

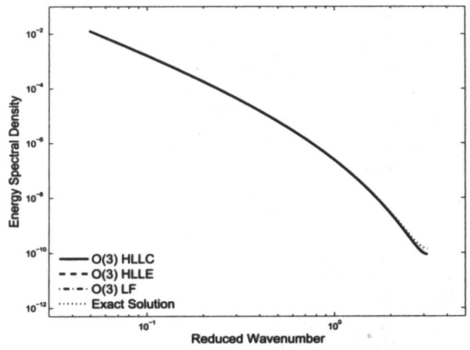

(a)

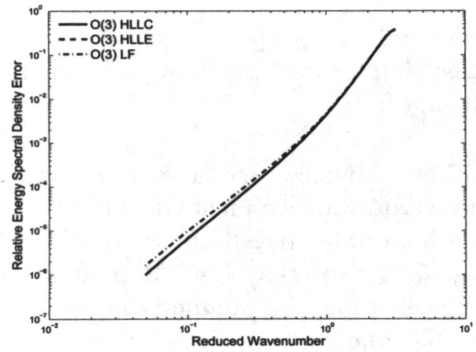

(b)

Figure 6: Energy spectral density (top) and relative energy spectral density error (bottom) from third-order simulations of the Euler simple wave problem. No limiter was used in all simulations shown.

dissipative, and all schemes have similar dissipation at the highest wavenumbers. What is not predicted is that the LF solution also has significantly greater dissipation at the low wavenumbers. The HLLE and HLLC-G solutions cannot be distinguished from each other at the scale of the plot as these Riemann solvers are very similar to each other in the absence of contact discontinuities. Here we have not presented the results for third order scheme using limiters. This is because third order methods perform badly with limiter. We refer to [23] for more details. Spectra from fourth-order simulations of the simple wave problem are shown in Fig. 7. Contrary to the predicted behavior, the LR limited (unlimited in this case) LF and HLLC solutions are indistinguishable. This lends

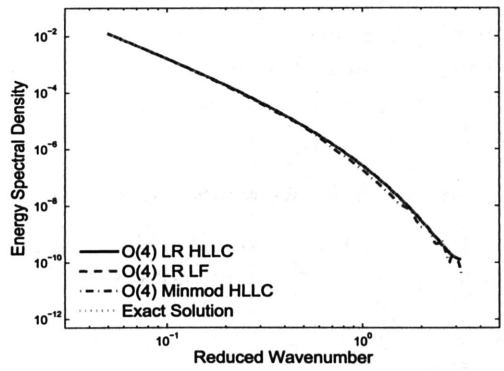

Figure 7: Energy spectral density from fourth-order simulations of the Euler simple wave problem.

credence to the idea that as the order of a scheme increases, the accuracy of the Riemann solver becomes less significant, at least for smooth problems. The minmod limited scheme also approximates the spectra reasonably, even though the solution is limited on almost all elements.

Conclusion

The spectral properties of RKDG schemes were investigated by computing their approximate modified wavenumber behavior and by comparing numerically obtained spectra for the simple wave problem to that of the exact solution. The modified wavenumber behavior of high-order unlimited RKDG schemes was found to be excellent. In particular, the dispersive performance of the fourth-order scheme is remarkably good, with very little deviation from spectral behavior over the complete range of numerically resolved wavenumbers. The dissipation of this scheme is also very low, even at the highest wavenumbers. This indicates that in regions away from discontinuities, where no limiting is required, RKDG schemes provide the high accuracy and low numerical dissipation needed, for example, to carry out LES simulations. This behavior was confirmed by spectra from the simple wave problem. When limiting is required, however, the spectral performance of RKDG schemes tends to that of the first-order method at high wavenumbers. Thus in the vicinity of discontinuities, high-order RKDG methods exhibit high numerical dissipation, similar

to that of second-order finite volume methods. In this region they are inferior to high-order WENO schemes that have been shown to provide improved modified wavenumber behavior. This is because the reconstructed numerical solution is always a high-order polynomial in the WENO schemes. This situation can only be improved by the development of high-order limiter functions for RKDG methods.

Acknowledgement The authors would like to acknowledge C. Schwab, M. Torrilhon and R. Hiptmair for their support and constructive discussions on this work. G. E. Karniadakis provided the authors with the original version of Nektar.

References

[1] G. Chavent, and B. Cockburn, The local projection p^0 p^1-discontinuous Galerkin finite element method for scalar conservation law, *Math. Model. Numer. Anal. (M^2AN)*, **23**, 1989, 565-592.

[2] B. Cockburn, S. Hou and C. W. Shu, The Runge-Kutta local projection discontinuous Galerkin finite element method for conservation laws IV:the multidimensional case, *Math. Comp.*, **54**, 1990, 545-581.

[3] B. Cockburn, S. Y. Lin and C. W. Shu, TVB Runge-Kutta local projection discontinuous Galerkin finite element method for conservation laws III:one dimensional systems, *J. Comp. Phys.*, **84**, 1989, 90-113.

[4] B. Cockburn and C. W. Shu, TVB Runge-Kutta local projection discontinuous Galerkin finite element method for conservation laws II:general framework, *Math. Comp.*,**52**, 1989, 411-435.

[5] B. Cockburn and C. W. Shu, The Runge-Kutta local projection P1-discontinuous Galerkin finite element method for scalar conservation laws, *Math. Model. Numer. Anal. (M^2AN)*, **25** 1991, 337-361.

[6] Cockburn, B. and Shu, C. W., *The Runge-Kutta local projection discontinuous Galerkin finite element method for conservation laws V:the multidimensional systems case*, J. Comp. Phys., Vol. 141, 1998, 199-224.

[7] B. Cockburn and C. W. Shu, The Runge-Kutta local projection p^1-discontinuous Galerkin method for scalar conservation laws, *M^2AN*, **25**, 1991, 337-361.

[8] M. Dubiner, Spectral methods on triangles and other domains, *J. Sci. Comp.*, **6**, 1991, 345-390.

[9] sperr H. Goedbloed and S. Poedts, *Principles of Magnetohydrodynamics*, Cambridge University Press, 2004.

[10] Hill, D. J. and Pullin, D. I., *Hybrid tuned center-difference-WENO method for large eddy simulations in the presence of strong shocks*, J. Comp. Phys., Vol 194, 2004, 435-450.

[11] Hill, T. R. and Reed, W. H., *Triangular mesh methods for neutron transport equation*, Los Alamos Scientific Laboratory Report LA-UR-73-479, 1973.

[12] Jiang, G. and Shu, C. W., *Efficient implimentation of weighted ENO schemes*, J. Comp. Phys, Vol. 126, 1996, 202-228 .

[13] Johnson C. and Pitkaranta, J., *An analysis of discontinuous Galerkin method for scalar hyperbolic equation*, Math. Comp., Vol. 26, 1986, 1-26.

[14] Karniadakis, G. E., and Sherwin, S. J., *Spectral/hp Element Methods for Computational Fluid Dynamics*, Oxford University Press, 2005.

[15] L. D. Landau and E. M. Lifshitz, *Fluid Mechanic, Chapter 101, Butterworth-Heinemann*, 2nd edn., 1987, 378.

[16] P. LeSaint and P. A. Raviart, On a finite element method for solving neutron transport equation, *Mathematical aspects of finite element in partial differential equations* (C. de Boor, Ed.), Academics Press, 1974, 89-145.

[17] G. Lin and G. E. Karniadakis, A discontinuous Galerkin Method for Two-Temperature Plasmas, *Comp. Meth. in Appl. Mech. and Eng.*, **195**, 2006, 3504-3527.

[18] T. Peterson, A note on the convergence of discontinuous Galerkin method for a scalar hyperbolic equation, *SIAM J. Numer. Anal.*, **28**, 1991, 133-140.

[19] S. Pirozzoli, On the spectral properties of shock-capturing schemes., *J. Comp. Phys.*, **219**, 2006, 489-497.

[20] S. J. Sherwin and G. E.Karniadakis, A new triangular and tetrahedral basis for high-order(hp) finite element methods, *Int. J. Numer. Methods. Eng.*, **123**, 1995 , 3775-3802.

[21] C. W. Shu, and S. Osher, Efficient implementation of essentially non-oscillatory shock capturing schemes, *J. Comp. Phys.*, **77**, 1988, 439-471.

[22] C. W. Shu, TVD time discretizations, *SIAM J. Math. Anal.*, **14**, 1988, 1073-1084.

[23] V. Wheatley, H. Kumar, P. Huguenot, On the Role of Riemann Solvers in Discontinuous Galerkin Methods for Magnetohydrodynamics, *J. Comp. Phys.* ,**229**, 2010, 660-680.

[1] *Mechanical Engineering*
University of Queensland
Brisbane
AUSTRALIA
E-mail: v.wheatley@uq.edu.au

[2] *Seminar for Applied Mathematics*
ETH Zurich
SWITZERLAND

[3] *Seminar for Applied Mathematics*
ETH Zurich
SWITZERLAND
E-mail: rolf.jeltsch@sam.math.ethz.ch